We are IntechOpen, the world's leading publisher of Open Access books
Built by scientists, for scientists

6,900
Open access books available

186,000
International authors and editors

200M
Downloads

Our authors are among the

154
Countries delivered to

TOP 1%
most cited scientists

12.2%
Contributors from top 500 universities

CLARIVATE ANALYTICS
BOOK CITATION INDEX
INDEXED

WEB OF SCIENCE™

Selection of our books indexed in the Book Citation Index
in Web of Science™ Core Collection (BKCI)

Interested in publishing with us?
Contact book.department@intechopen.com

Numbers displayed above are based on latest data collected.
For more information visit www.intechopen.com

Bio and Chemical Sensors Based on Surface Plasmon Resonance in a Plastic Optical Fiber

Nunzio Cennamo and Luigi Zeni

Additional information is available at the end of the chapter

1. Introduction

Surface Plasmon Resonance (SPR) is known to be a very sensitive technique for determining refractive index variations at the interface between a metallic layer and a dielectric medium (analyte). SPR is widely used as a detection principle for many sensors operating in different application fields, such as bio and chemical sensing. In practical implementations, the biological targets are usually transported through a microfluidic system by means of a buffer fluid or a carrier fluid. In SPR sensors, the transducing media (ligands) are usually bonded on the metallic layer surface so that, when they react with the target molecules present in the analyte, the refractive index at the outer interface changes, and this change is detected by suitable optical interrogation. In the scientific literature, many different configurations based on SPR in silica optical fibers, are usually found [1,2].

In general, the optical fiber employed is either a glass one or a plastic one (POF). For low-cost sensing systems, POFs are especially advantageous due to their excellent flexibility, easy manipulation, great numerical aperture, large diameter, and the fact that plastic is able to withstand smaller bend radii than glass. The advantages of using POFs is that the properties of POFs, that have increased their popularity and competitiveness for telecommunications, are exactly those that are important for optical sensors based on optical fibers. Moreover, a further advantage of POF sensors is that they are simpler to manufacture than those made using silica optical fibers. In the scientific literature only simple POF sensors, based on laterally polished bent sections prepared along a plastic optical fiber, can be usually found.

In this chapter, POF sensor configurations are presented in order to monitor an aqueous environment (refractive index around 1.333), with a resolution ranging from 10^{-4} to 10^{-3} (RIU). The classic geometries of sensors based on SPR in silica optical fiber are adapted and borrowed for POF, so representing a simple approach to low cost plasmonic sensing.

The planar gold layer of the sensors, the low resolution and refractive index ranging from 1.332 to 1.420 are three good factors for forthcoming bio/chemical sensors implementation.

Another aspect to be considered is that most often the SPR bio-chemical sensor system is based on a high refractive index prism coated with a thin metallic layer. The incidence angle of the light can be changed in a wide range and, as a consequence, the surface plasma waves (plasmons) may exist whatever the surrounding medium, i.e. a gas or a liquid. These sensors are usually bulky and require expensive optical equipment, not easy to be miniaturized. In addition, the remote sensing can be very difficult to exploit. On the contrary, the use of a POF makes the remote sensing straightforward, and may reduce the cost and dimension of the device, with the possibility of integration of SPR sensing platform with optoelectronic devices, eventually leading to "Lab-on-a-chip".

2. SPR phenomenon

In the optical phenomenon of Surface Plasmon Resonance, a metal-dielectric interface supports a p-polarized electromagnetic wave, namely Surface Plasmon Wave (SPW), which propagates along the interface. When the p-polarized light is incident on this metal-dielectric interface in such a way that the propagation constant (and energy) of resultant evanescent wave is equal to that of the SPW, a strong absorption of light takes place as a result of transfer of energy and the output signal exhibits a sharp dip at a particular wavelength known as the resonance wavelength. The so-called resonance condition is given by the following expression:

$$K_0 n_c \sin \vartheta = K_0 \left(\frac{\varepsilon_{mr} n_s^2}{\varepsilon_{mr} + n_s^2}\right)^{1/2}; \quad K_0 = \frac{2\pi}{\lambda} \tag{1}$$

The term on the left-hand side is the propagation constant K_{inc} of the evanescent wave generated as a result of Attenuated Total Reflection (ATR) of the light incident at an angle θ through a light coupling device (such as prism or optical fiber) of refractive index n_c. The right-hand term is the SPW propagation constant (K_{SP}) with ε_{mr} as the real part of the metal dielectric constant (ε_m) and n_s as the refractive index of the sensing (dielectric) layer. This matching condition of propagation constants is heavily sensitive to even a slight change in the dielectric constant, which makes this technique a powerful tool for sensing of different parameters.

2.1. Spectral mode operation

In SPR sensors with spectral interrogation, the resonance wavelength (λ_{res}) is determined as a function of the refractive index of the sensing layer (n_s). If the refractive index of the sensing layer is altered by δ_{ns}, the resonance wavelength shifts by $\delta\lambda_{res}$. The sensitivity (S_n) of an SPR sensor with spectral interrogation is defined as [3]:

$$S_n = \frac{\delta\lambda_{res}}{\delta n_s} \left[\frac{nm}{RIU} \right] \tag{2}$$

Owing to the fact that the vast majority of the field of an SPW is concentrated in the dielectric, the propagation constant of the SPW is extremely sensitive to changes in the refractive index of the dielectric itself. This property of SPW is the underlying physical principle of affinity SPR bio/chemical sensors. In the case of artificial receptors, as molecular imprinted polymers (MIPs), the polymeric film on the surface of metal selectively recognizes and captures the analyte present in a liquid sample so producing a local increase in the refractive index at the metal surface. The refractive index increase gives rise to an increase in the propagation constant of SPW propagating along the metal surface which can be accurately measured by optical means. The magnitude of the change in the propagation constant of an SPW depends on the refractive index change and its overlap with the SPW field. If the binding occurs within the whole depth of the SPW field, the binding-induced refractive index change produces a change in the real part of the propagation constant, which is directly proportional to the refractive index change.

The resolution (Δn) of the SPR-based optical sensor can be defined as the minimum amount of change in refractive index detectable by the sensor. This parameter (with spectral interrogation) definitely depends on the spectral resolution ($\delta\lambda_{DR}$) of the spectrometer used to measure the resonance wavelength in a sensor scheme. Therefore, if there is a shift of $\delta\lambda_{res}$ in resonance wavelength corresponding to a refractive index change of δn_s, then resolution can be defined as:

$$\Delta n = \frac{\delta n_s}{\delta\lambda_{res}} \delta\lambda_{DR} \left[RIU \right] \tag{3}$$

The Signal-to-Noise Ratio of an SPR sensor depends on how accurately and precisely the sensor can detect the resonance wavelength and hence, the refractive index of the sensing layer. This accuracy in detecting the resonance wavelength further depends on the width of the SPR curve.

The narrower the SPR curve, the higher the detection accuracy. Therefore, if $\delta\lambda_{SW}$ is the spectral width of the SPR response curve corresponding to some reference level of transmitted power, the detection accuracy of the sensor can be assumed to be inversely proportional to $\delta\lambda_{SW}$.

The signal-to-noise ratio of the SPR sensor with spectral interrogation is, thus, defined as:

$$SNR(n) = \left(\frac{\delta\lambda_{res}}{\delta\lambda_{SW}} \right)_n \tag{4}$$

where $\delta\lambda_{SW}$ can be calculated as the full width at half maximum of the SPR curve (FWHM). SNR is a dimensionless parameter strongly dependent on the refractive index changes.

2.2. Amplitude mode operation

In SPR sensors, it can be used a simpler scheme with a monochromatic light source and an optical power meter in the amplitude mode operation, because in the shoulders of spectral response curve, appreciable intensity differences are present, as the given refractive index changes, due to the shift of the curve itself.

In amplitude mode operation the sensitivity (S_n) of an SPR sensor is defined as:

$$S_n = \frac{\delta I_{norm}}{\delta n_s} \left[\frac{a.u.}{RIU} \right]$$ (5)

where I_{norm} is the relative output, normalized to a reference level, in order to compensate for light source fluctuations.

The resolution (Δn) of the SPR-based optical sensor, in amplitude mode operation, can be defined as:

$$\Delta n = \frac{\delta n_s}{\delta I_{norm}} \ \sigma \left[RIU \right]$$ (6)

where σ is the standard deviation of the relative output.

3. A POF sensor system for biosensor implementation

The fabricated optical sensor system was realized removing the cladding of a plastic optical fiber along half the circumference, spin coating on the exposed core a buffer of Microposit S1813 photoresist, and finally sputtering a thin gold film using a sputtering machine [4].

The plastic optical fiber has a PMMA core of 980 μm and a fluorinated polymer cladding of 20 μm. The experimental results indicate that the configuration with a fiber diameter of 1000 μm exhibits better performance in terms of sensitivity and resolution but not in terms of SNR [5], as shown in section 5.2.

The refractive index, in the visible range of interest, is about 1.49 for PMMA, 1.41 for fluorinated polymer and 1.61 for Microposit S1813 photoresist. The sample consisted in a plastic optical fiber without jacket embedded in a resin block, with the purpose of easing the polishing process. The polishing process was carried out with a 5 μm polishing paper in order to remove the cladding and part of the core. After 20 complete strokes following a "8-shaped" pattern (according to the manufacturer recommendations, as shown in Figure 1) in order to completely expose the core, a 1 μm polishing paper was used for another 20 complete strokes following a "8-shaped" pattern. The realized sensing region was about 10 mm in length.
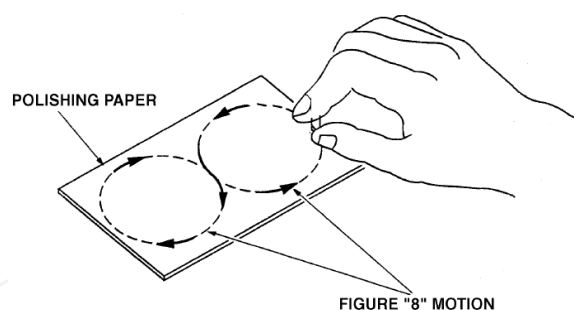
Figure 1. "8-shaped" pattern for POF polishing.

The buffer of Microposit S1813 photoresist was realized by means of spin coating. The Microposit S1813 photoresist is deposited in one drop (about 0.1 ml) on the center of the substrate. The sample is then spun at 6,000 rpm for 60 seconds. The final thickness of photoresist buffer was about 1.5 μm.

As it will be shown in the section 5.1, the experimental results indicate that this configuration with the photoresist buffer layer exhibits better performance in terms of detectable refractive index range and SNR [4].

Finally, a thin gold film was sputtered by using a sputtering machine (Bal-Tec SCD 500).The sputtering process was repeated twice with a current of 60 mA for a time of 35 seconds (20 nm for step). The gold film so obtained was 60 nm thick and presented a good adhesion to the substrate, verified by its resistance to rinsing in de-ionized water.

This sensor based on SPR in a POF is a common tool for surface interaction analysis and biosensing, widely used as a detection principle for sensors that operate in different areas of bio and chemical sensing as reported in several recent review papers [6,7]. In this case on the gold surface there is a bio or chemical layer for the selective detection and analysis of analyte in aqueous solution (see figure 2).
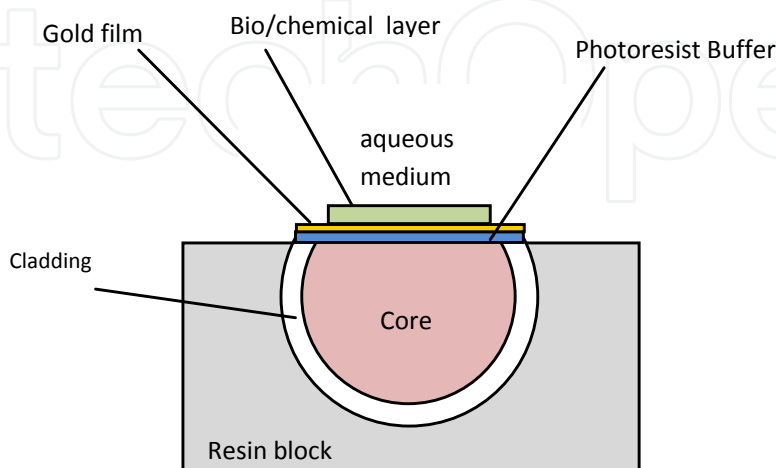

Figure 2. Section of POF sensor

4. Experimental configurations for SPR sensors in plastic optical fibers

The experimental measurements for the characterization of the POF sensor, presented in the previous section, were carried out in two different ways: spectral and amplitude mode. Figure 3 shows the experimental setup arranged to measure the transmitted light spectrum and was characterized by a halogen lamp, illuminating the optical sensor system, and a spectrum analyzer. The employed halogen lamp exhibits a wavelength emission range from 360 nm to 1700 nm, while the spectrum analyzer detection range was from 200 nm to 850 nm. The spectral resolution of the spectrometer was 1.5 nm (FWHM).
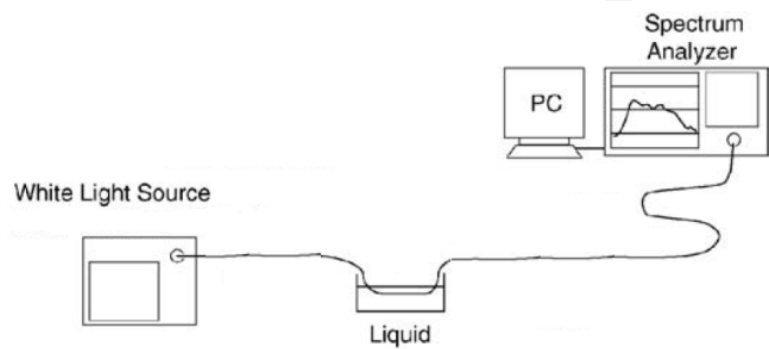
Figure 3. Setup to measure the transmitted light spectrum

Figure 4 shows the measurements carried out, obtaining SPR transmission spectra, normalized to the spectrum achieved with air as the surrounding medium, for three different water-glycerin solutions with refractive index 1.333, 1.351, 1.371, respectively. The sensitivity is calculated as the slope of the resonance wavelength versus refractive index curve, for three refractive index values. In figure 5 the experimental data and the linear fitting are presented.
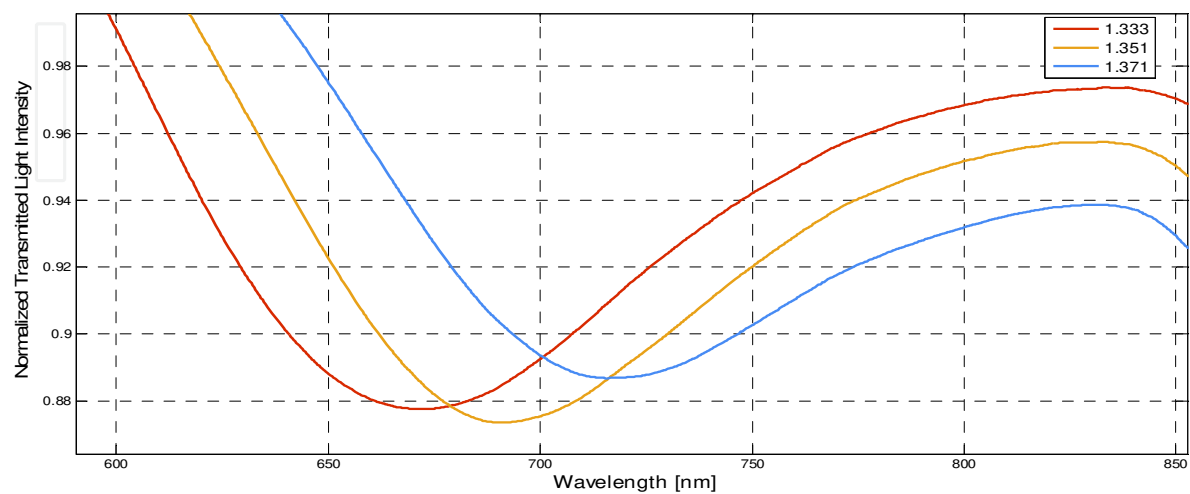
Figure 4. Normalized transmitted light intensity as function a function of the wavelength
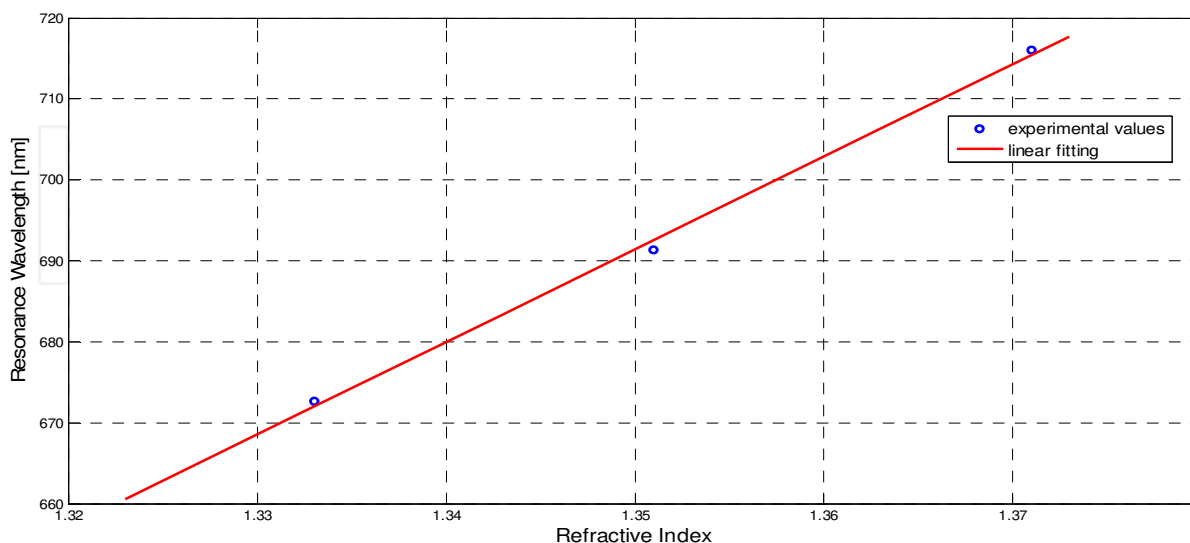
Figure 5. Resonance wavelength as a of the refractive index

Figure 6 shows the second setup. It is composed of an LED, whose wavelength is 670nm, as the light source, a beam splitter, two photodiodes whose function is to convert the light into an electrical signal and an oscilloscope for signal acquisition connected to a PC.

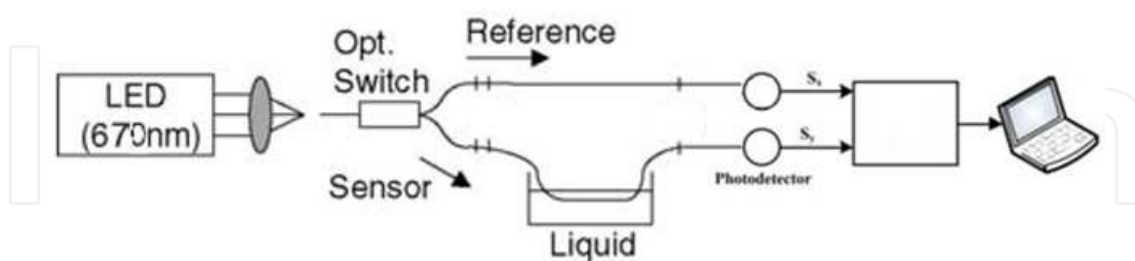In figure 7, the relative output is plotted as a function of time for three different refractive index values.

Figure 6. Setup using a LED and two photodiode

According to an experiment for the evaluation of system stability, the standard deviation of the relative output was found to be 3.84×10^{-4} for the 8 min continuous operation in the air with the intention of circumventing liquid evaporation. In figure 8, the relative output for three different refractive index and the linear fitting to the experimental values are presented.
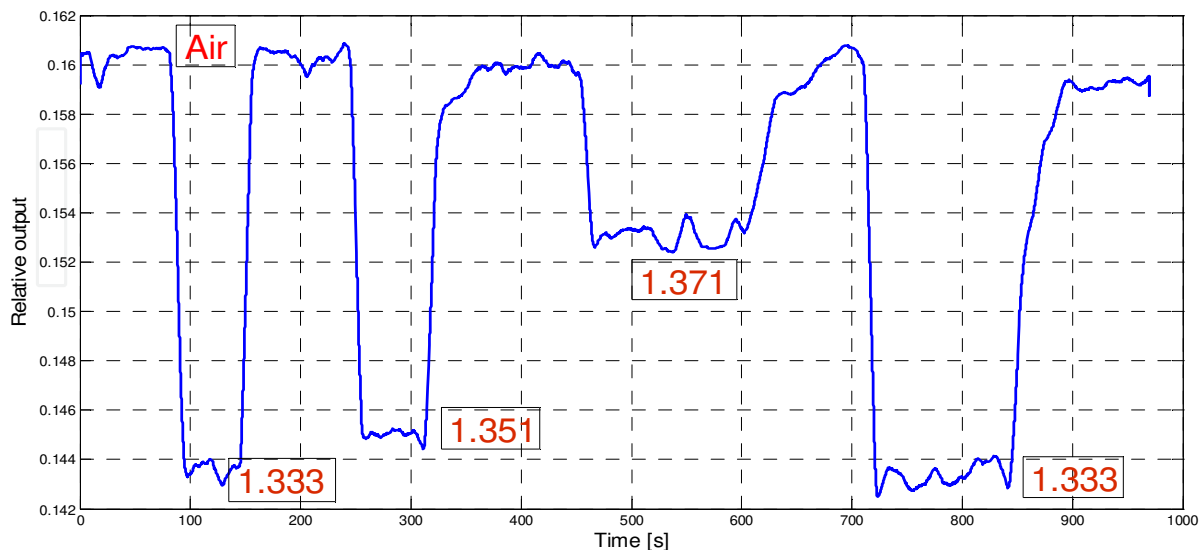
Figure 7. Relative output as a function of time, for different refractive index values
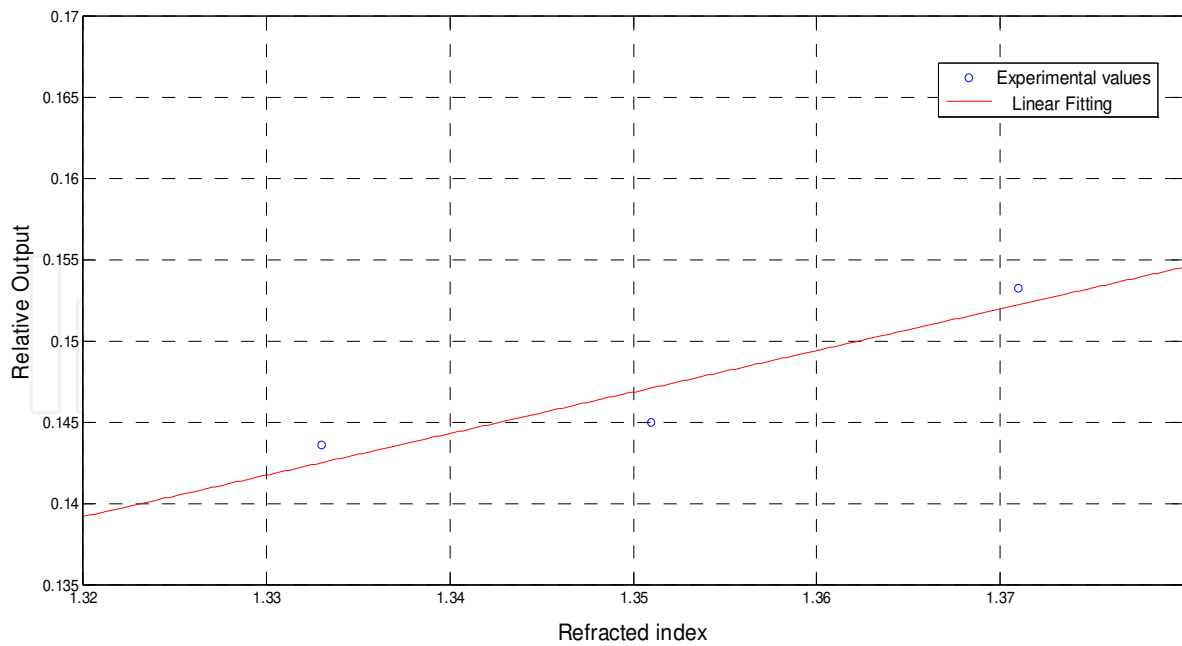

Figure 8. Relative output as a function of refractive index

For a clearer comparative analysis of the two experimental setups, table 1 summarizes the average values of the experimentally measured performance parameters, evaluated by Matlab software, for external medium refractive index ranging from 1.333 to 1.371.

Experimental setup	Sensitivity (S)	Margin of error (∂E)	Δn = S⁻¹ * ∂E
White Light Source/ spectrum analyzer	$\frac{\delta\,resonance\,wavelength}{\delta\,refractive\,index}=1.14*10^3\left[\frac{nm}{RIU}\right]$	(spectral resolution of the spectrometer) 1.5 nm (FWHM)	0.00131 [RIU]
LED/photodiodes	$\frac{\delta\,relative\,output}{\delta\,refractive\,index}=0.26\left[\frac{a.u.}{RIU}\right]$	(standard deviation) 3.84×10^{-4}	0.00147 [RIU]

Table 1. Performance parameters for different experimental configurations

5. Performance comparison of sensors based on SPR in POF

In this section different POF sensor configurations are presented and experimentally tested with spectral interrogation: First, the configurations with and without photoresist buffer layer; then, the configurations with two different POF core diameters and finally the configuration with a tapered POF.

5.1. POF sensors with and without the photoresist layer

In this section we present two configurations with and without the photoresist buffer layer (see figure 2). In the series of performed experiments, water-glycerin solutions were used to achieve an aqueous medium with variable refractive index. Without the buffer layer, in the same operating conditions, the sensor is capable of monitoring refractive indexes ranging from 1.330 to 1.360. In Figure 9 are presented the experimentally obtained SPR transmission spectra, normalized to the spectrum achieved with air as the surrounding medium, for three different water-glycerin solutions with refractive index ranging from 1.332 to 1.352.

In the presence of the photoresist buffer layer, the refractive index range is increased. In particular, this fiber optic sensor is capable of monitoring an aqueous environment whose refractive index ranges from 1.332 to 1.418.

In Figure 10 are presented the experimentally obtained SPR transmission spectra, normalized to the spectrum achieved with air as the surrounding medium, obtained in this case with the photoresist buffer layer, for different water-glycerin solutions with refractive index ranging from 1.332 to 1.418.

In presence of the photoresist buffer layer, the refractive index range is increased while the sensitivity is the same.
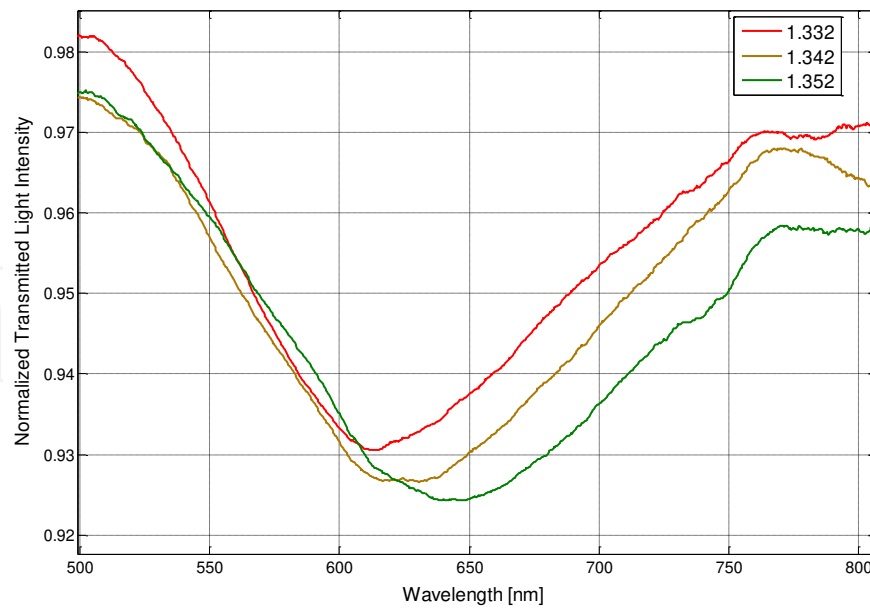
Figure 9. Experimentally obtained SPR transmission spectra, normalized to the air spectrum, for different refractive index of the aqueous medium. Configuration without the photoresist buffer layer.
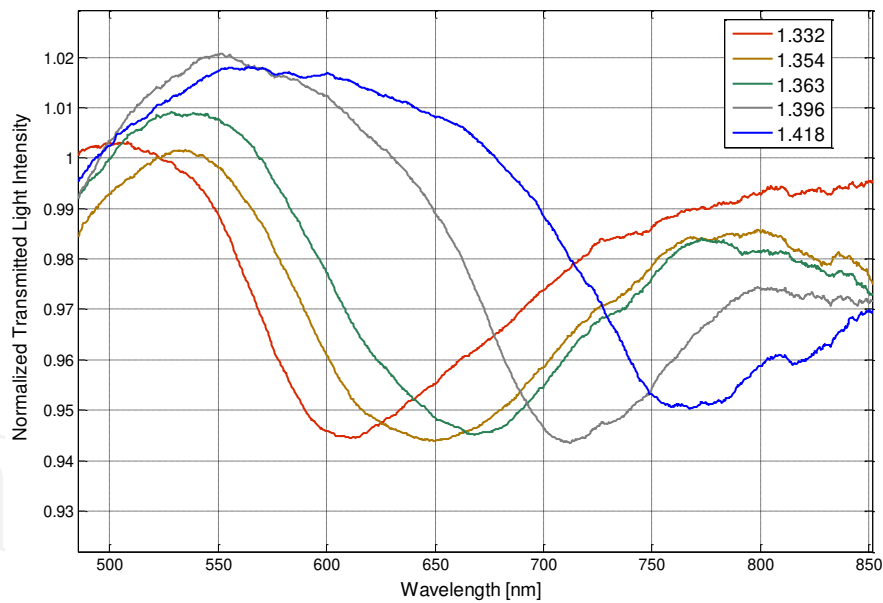

Figure 10. Experimentally obtained SPR transmission spectra, normalized to the air spectrum, for different refractive index of the aqueous medium. Configuration with the photoresist buffer layer.

Without the photoresist buffer layer there is a decrease in the power transmitted to the fiber end facet, due to a greater dissipation. This decrease results in the decrease of the SPR curve and the increase of the SPR curve width. Therefore, it can be conveniently established that SPR curve width increases ($\delta\lambda_{SW}$) without the photoresist buffer layer, as shown for example in Figure 11 for a refractive index equal to 1.332 (water).
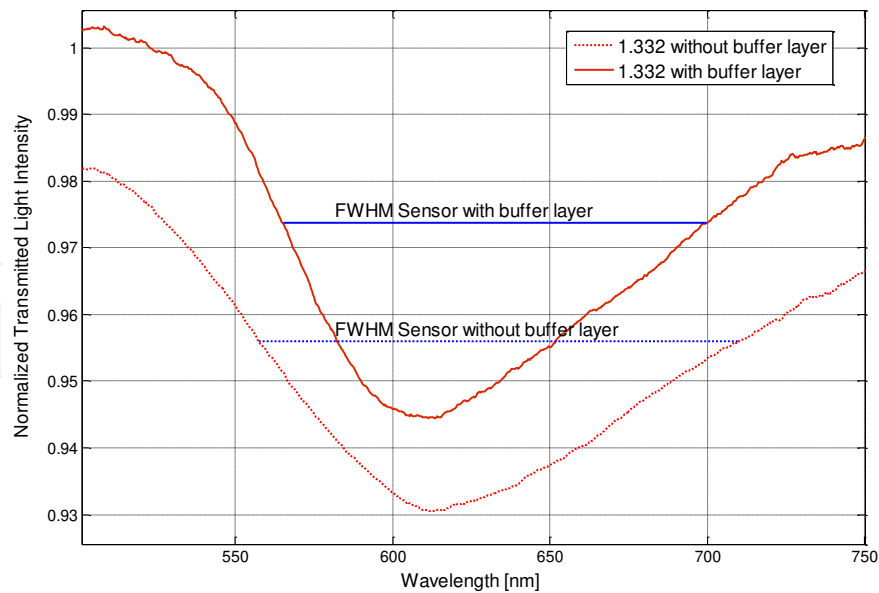
Figure 11. The full width at half maximum (FWHM) of the SPR curve for the two sensors configurations with and without the buffer layer for an external refractive index of 1.332.

The observed absorption band is the result of the convolution of different resonance peaks. Each peak is obtained for a specific resonance condition defined by a given angle-wavelength couple. Therefore, the experimental results indicate that the configuration with the photoresist buffer layer exhibits better performance in terms of detectable refractive index range and SNR.

5.2. POF sensors with two different POF core diameters

In this section we presented the influence of POF core diameter on sensor performances. Before entering the details of the discussion, as a similar analysis is present in the literature with reference to a sensor based SPR in silica optical fiber without any buffer layer between the fiber core and the gold film [8], it is convenient to briefly recall some fundamental aspects of light rays propagation in optical fibers where surface plasmons are excited.

Inside an optical fiber, any light ray making an angle θ from the normal to core-cladding interface undergoes multiple reflections (N_{ref}), depending on the length of SPR sensing region (L) and fiber core diameter (D), according to the following relation [8]:

$$N_{ref}(\theta) = \frac{L}{D \tan \theta} \tag{7}$$

To determine the effective transmitted power, the reflectance (R_e) for a single reflection is raised to the power equal to corresponding number of reflections. Therefore, the generalized expression (all guided rays) for the normalized transmitted power (P_{trans}) in sensors based on SPR in fiber optic can be written as:

$$P_{trans} = \frac{\int_{\theta cr}^{\pi/2} R_e^{N_{ref}(\theta)} I(\theta) d\theta}{\int_{\theta cr}^{\pi/2} I(\theta) d\theta} \qquad (8)$$

In Equation (8), $I(\theta)$ is the angular intensity distribution corresponding to the light source used. Further, θ_{cr} is the critical angle of the fiber, which heavily depends on the Numerical Aperture (NA) of the fiber and light wavelength.

The angular range from θ_{cr} to $\pi/2$ covers whole range of guided rays (or modes) as these angles correspond to the highest order mode and the fundamental mode of an optical fiber, respectively. The number of modes that can propagate in a fiber depends on the fiber's Numerical Aperture (or acceptance angle) as well as on its core diameter and the wavelength of the light. For a step-index multimode fiber, the number of such modes, M, is approximated (M >> 1) by:

$$M \cong 0.5 * \left(\frac{\pi * D * NA}{\lambda} \right)^2 \qquad (9)$$

where D is the core diameter, λ is the operating wavelength, NA is the Numerical Aperture (or acceptance angle, as shown in Figure 12).
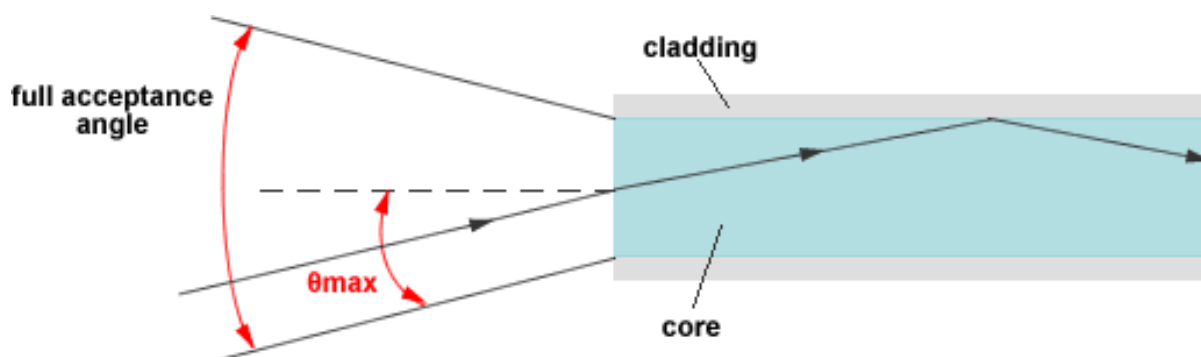

Figure 12. Optical fiber acceptance cone.

In general, numerical aperture of a Plastic Optical Fiber is greater than that of a Silica Optical Fiber. The resonance condition (see Equation (1)) is satisfied at different wavelengths depending on which combination of core diameter and sensing region length is considered. It is so clear that the performance parameters of a fiber optic SPR sensor strictly depend on the values of design parameters such as fiber core diameter (D), sensing region length (L), and numerical aperture (NA). In this section, we analyze the influence of two values of Plastic Optical Fiber core diameter (D) on the performance of a sensor based on Surface Plasmon Resonance in a POF, where the sensing region length is fixed and a photoresist buffer layer is placed between the fiber core and the gold film (see figure 2).

For sensors based on SPR in optical fiber (silica or plastic) the shift in resonance wavelength ($\delta\lambda_{res}$), for a fixed refractive index variation (δn_s), increases with a decrease in the number of reflections. Therefore, sensitivity increases with the increase of fiber core diameter and with the decrease of sensing region length.

Figure 13 reports the experimentally obtained SPR transmission spectra, when the diameter POF is 1,000 µm (figure 13 (a)) and 250 µm (figure 13 (b)), normalized to the spectrum achieved with air as the surrounding medium, for five different water-glycerin solutions with refractive index ranging from 1.332 to 1.372.
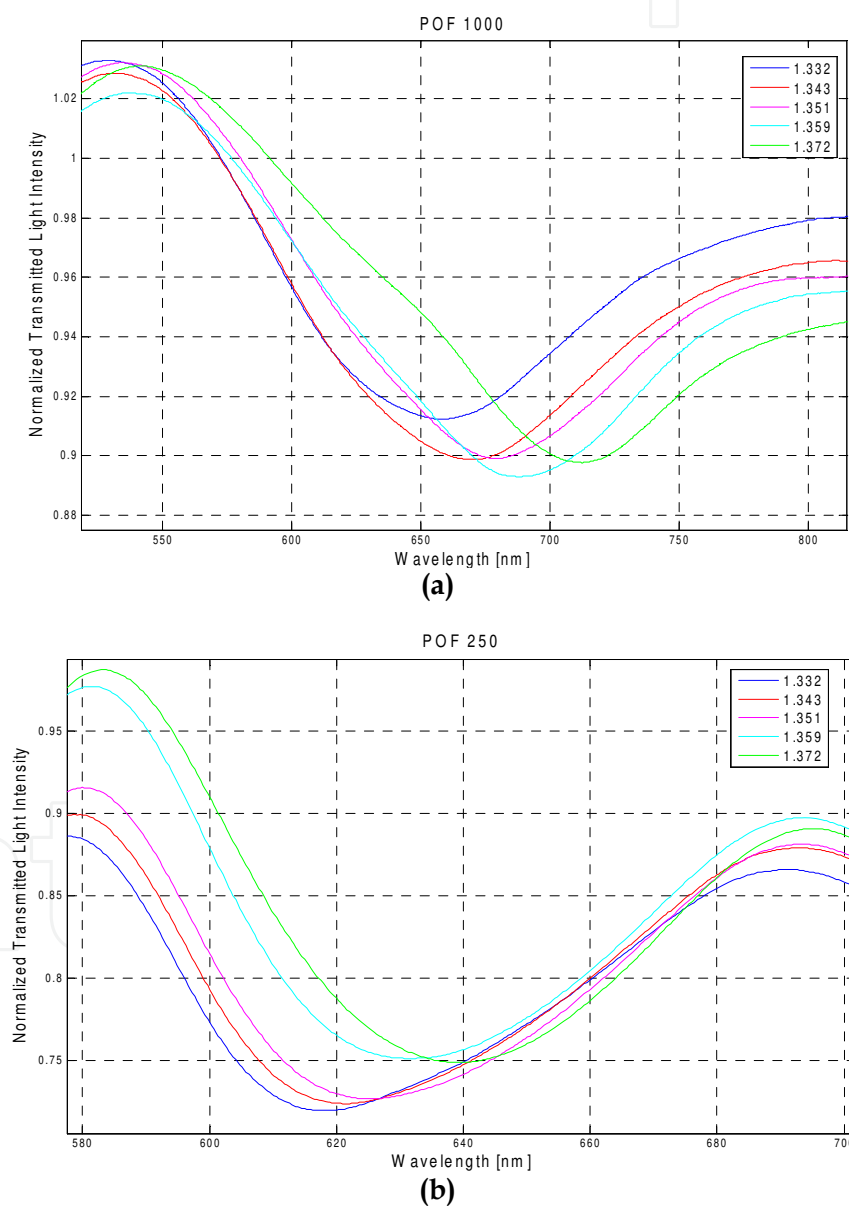

(a)

(b)

Figure 13. Experimentally obtained SPR transmission spectra, normalized to the air spectrum, for different refractive index of the aqueous medium. (a) Configuration with a 1,000 µm diameter POF; (b) Configuration with a 250 µm diameter POF

Figure 14 shows the resonance wavelength versus the refractive index obtained with the two different configurations. In the same figure is also presented the linear fitting to the experimental data, showing a good linearity for the sensors. The Pearson's correlation coefficient (R) is 0.99 for the sensor with a POF of 1,000 μm and 0.98 for the sensor with a POF of 250 μm diameter.

The sensitivity, as defined in Equation (2), is the shift of the resonance wavelength (nm) per unit change in refractive index (nm/RIU). Therefore, it is the angular coefficient of the linear fitting. Figure 14 shows as the sensitivity increases with the fiber core diameter.
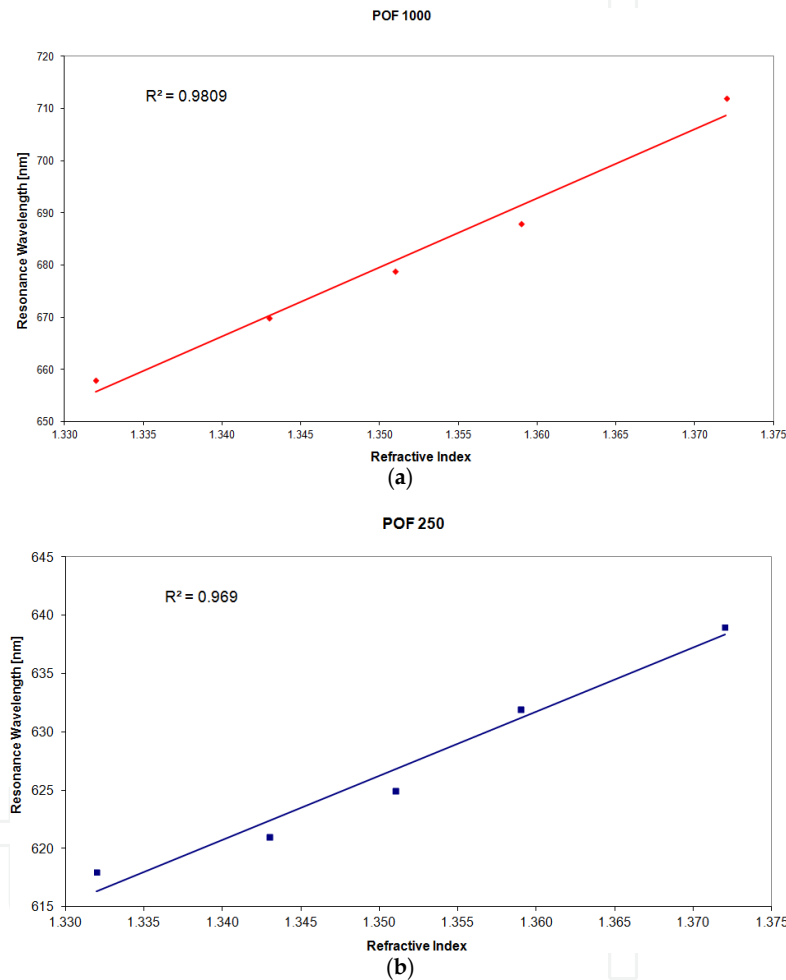

Figure 14. Plasmon resonance wavelength as a function of the refractive index. (a) Configuration with a 1,000 μm diameter POF. (b) Configuration with a 250 μm diameter POF.

Furthermore, as sensor's resolution also depends on the variation of $\delta\lambda_{res}$ (see Equation (3)), therefore, similarly to sensitivity, resolution also tends to improve for larger fiber core diameters (see Figure 15). In fact, the resolution (Δn) can be calculated as the angular coefficient of the linear fitting in Figure 15 multiplied to the spectral resolution ($\delta\lambda_{DR}$) of the spectrometer used to measure the resonance wavelength.
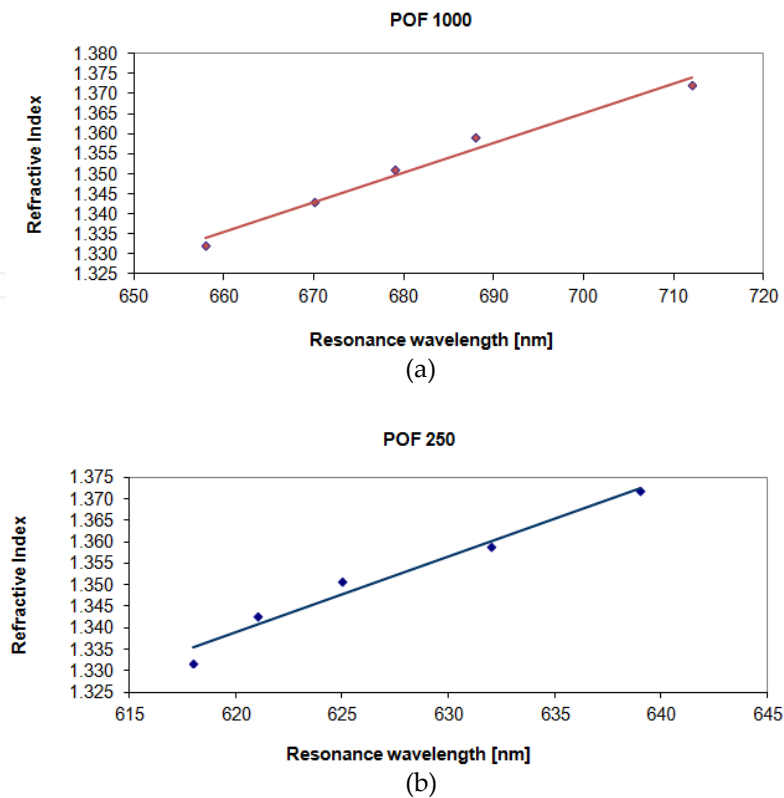
Figure 15. Refractive index as a function of the plasmon resonance wavelength. (a) Configurations with a 1,000 μm diameter POF. (b) Configurations with a 250 μm diameter POF.

The experimental results obtained with the two values of POF core diameter have shown as the Numerical Aperture of POF and the photoresist buffer layer have produced a different behavior with respect to many different configurations based on SPR in silica optical fibers, as SNR is concerned. From our experimental results [5], it is clear that the shift in resonance wavelength ($\delta\lambda_{res}$), for a fixed refractive index variation (δ_{ns}), increases when the core diameter increases. Therefore, sensitivity increases with an increase in fiber core diameter. Furthermore, in the sensors based on SPR in POF (configuration with the photoresist buffer layer) as already established, SPR curve width ($\delta\lambda_{SW}$) increases with an increase in fiber core diameter. There-fore, it can be conveniently established that SPR curve width increases ($\delta\lambda_{SW}$) with the increase of fiber core diameter, as shown in Figure 16 for a refractive index equal to 1.332.

SPR curve width $\delta\lambda_{SW}$ can be calculated as the full width at half maximum (FWHM) of the SPR curve. FWHM of the SPR curve as a function of the refractive index is shown in Figure 17. Therefore, SNR is expected to decrease because an increase in the shift in resonance wavelength ($\delta\lambda_{res}$) produces a larger increase in the curve width ($\delta\lambda_{SW}$), for a fixed increase in fiber core diameter.

More precisely, for a POF with 250 μm of diameter, the angular coefficient of the linear fitting shown in Figure 14 ($\delta\lambda_{res}$) is greater than the angular coefficient of the linear fitting shown in Figure 17 ($\delta\lambda_{SW}$). In this case SNR is greater than one. For a POF with 1,000 μm of diameter the angular coefficient of the linear fitting shown in Figure 14 ($\delta\lambda_{res}$) is lower than the angular coefficient of the linear fitting shown in Figure 17 ($\delta\lambda_{SW}$). In this case SNR is less than one.
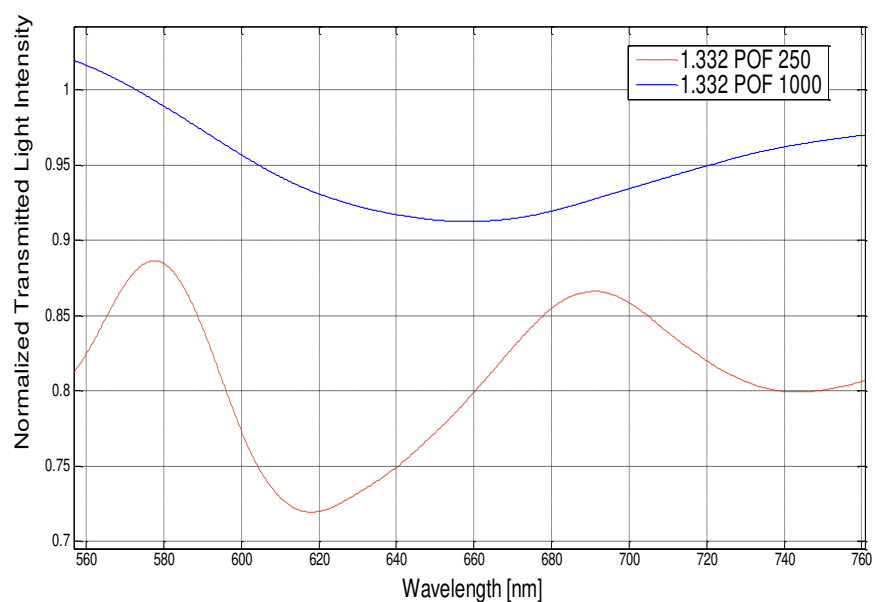
Figure 16. The full width at half maximum of the SPR curve for the two sensors configurations (250 μm and 1,000 μm POF diameter) for an external refractive index of 1.332.
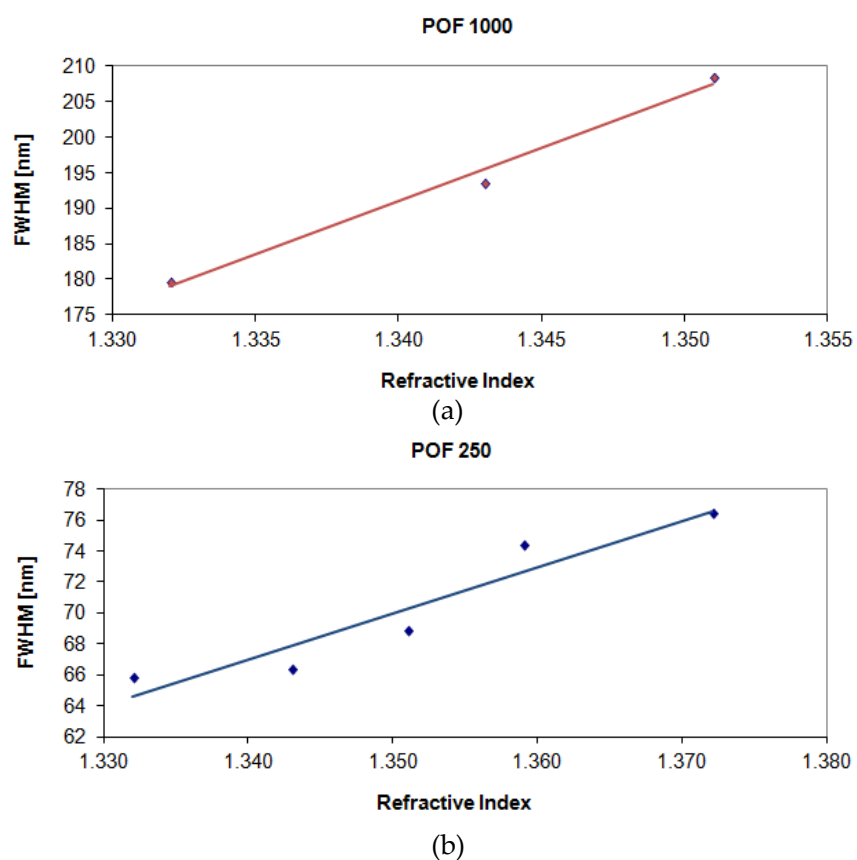

Figure 17. The full width at half maximum of the SPR curve as a function of the refractive index. (a) Configuration with a 1,000 μm diameter POF. (b) Configuration with a 250 μm diameter POF.

The plasmon resonance wavelength as a function of the full width at half maximum of the SPR curve is shown in Figure 18. SNR can be calculated as the angular coefficient of the linear fitting reported in Figure 18. From the above figure, it is clear that the SNR increases when the fiber core diameter decreases. It is important to emphasize that the calculation, from experimental data, of the single values of above parameters has been carried out by employing a first-order approach, while the linear fitting does not imply an actual linear relationship but it is just a way to extrapolate a trend and allow an easy comparison between the two sensor systems.
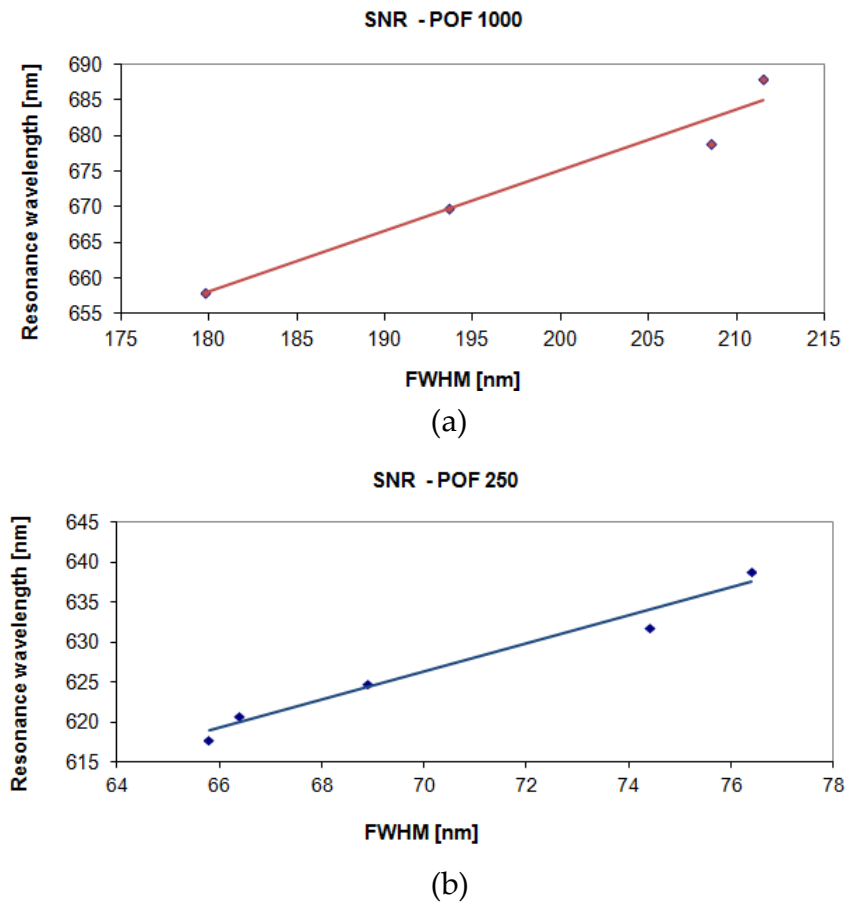

(a)

(b)

Figure 18. Plasmon resonance wavelength as a function of the full width at half maximum of the SPR curve. (a) Configuration with a 1,000 μm diameter POF. (b) Configuration with a 250 μm diameter POF.

For a clearer comparative analysis between the two sensors with 250 μm and 1,000 μm diameter POFs, Table 2 summarizes the averages values of the experimentally measured performance parameters, evaluated by Matlab software, for external medium refractive index ranging from 1.332 to 1.372.

POF Diameter [μm]	Resolution (Δn) [RIU]	Signal-to-noise ratio (SNR)	Sensitivity (S) [nm/RIU]	FWHM/Δn [nm/RIU]
250	0.0027	1.7548	0.549×10^3	0.298×10^3
1,000	0.0010	0.8569	1.325×10^3	1.495×10^3

Table 2. Performance comparison for the two sensors configurations: 250 μm and 1,000 μm diameter POF, respectively.

5.3. Sensor configuration with taperd POF

Figure 19 shows the optical sensor configuration with a tapered POF. The optical sensor can be realized removing the cladding of a plastic optical fiber along half circumference, heating and stretching it and finally sputtering a thin gold film.
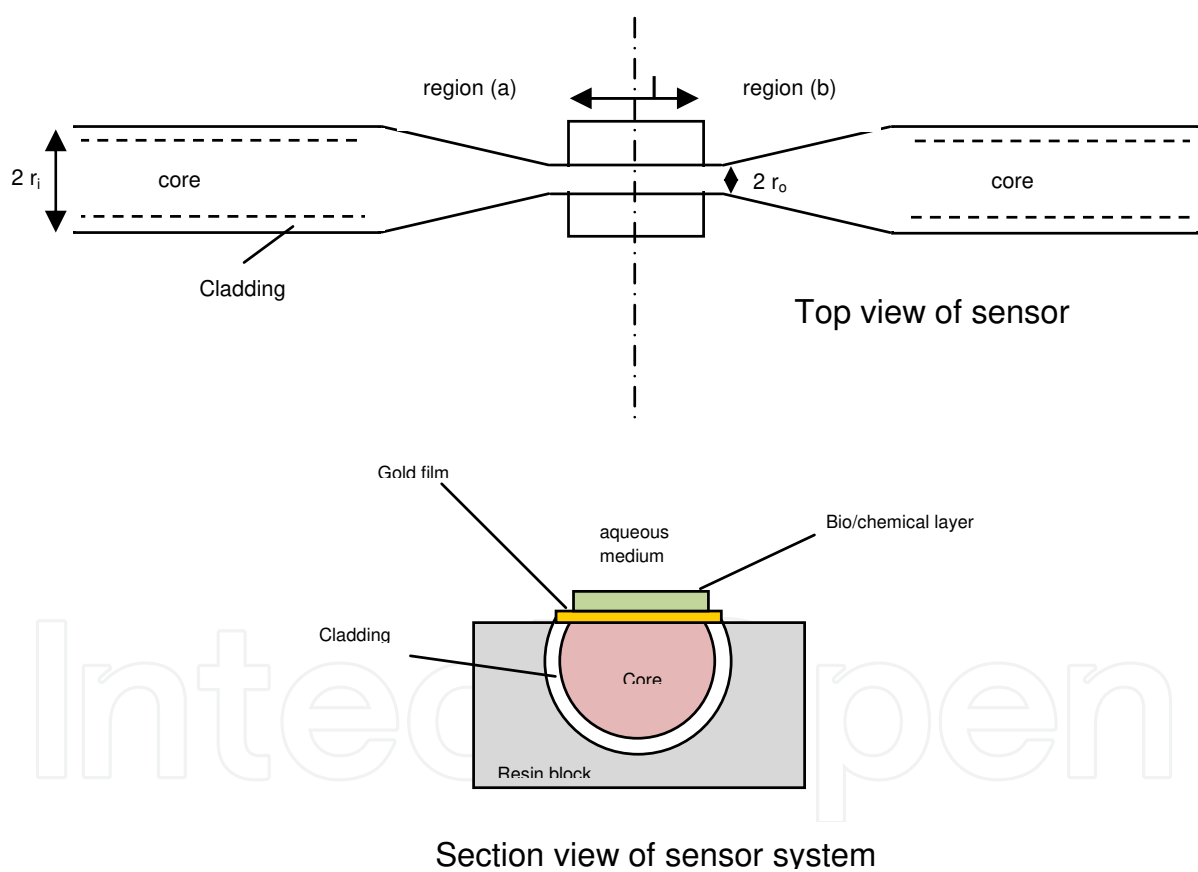

Figure 19. Sensor system based on SPR in tapered POF

The experimental results, presented in this section, are obtained with the following configuration: The plastic optical fiber has a PMMA core of 980 μm and a fluorinated cladding of 20μm. The taper ratio (r_i/r_o) is about 1.5 and the sensing region (L) is about 10 mm in length. The thicknesses of gold layer is about 60 nm. The sensor was realized starting from a plastic optical fiber, without protective jacket, heated (at 150°C) and stretched with a motorized linear

positioning stage until the taper ratio reached 1.5. After this step, the POF was embedded in a resin block, and polished with a 5 μm polishing paper in order to remove the cladding and part of the core. After 20 complete strokes following a "8-shaped" pattern in order to completely expose the core, a 1 μm polishing paper was used for another 20 complete strokes with a "8-shaped" pattern. The thin gold film was sputtered by using a sputtering machine (Bal-Tec SCD 500).The sputtering process was repeated three-time with a current of 60 mA for a time of 35 seconds (20 nm for step). On the top of planar gold film it is possible to apply a bio/chemical layer for the selective detection of analytes.

When SPR is achieved in optical fibers, the introduction of the tapered region (a) in fig. 19 helps to reduce the incidence angles of the guided rays in the fiber close to the critical angle of the unclad uniform tapered region. This is obtained by choosing the minimum allowed value of the radius of the output end of the taper so that all the rays remain guided in the uniform core sensing region [9]. After propagating through the uniform region the rays enter the tapered region (b) (see fig. 19) which reconverts the angles of these rays into their initial values so that they can propagate up to the output end of the fiber. Thus, the sensing probe has the minimum diameter such that no ray leaks out and a majority of rays are bound to propagate close to the critical angle, thereby increasing the penetration depth of the evanescent field to almost the maximum value [9].

Figure 20 reports the experimentally obtained SPR transmission spectra, obtained with this tapered POF configuration, normalized to the spectrum achieved with air as the surrounding medium, for six different water-glycerin solutions with refractive index ranging from 1.333 to 1.385.
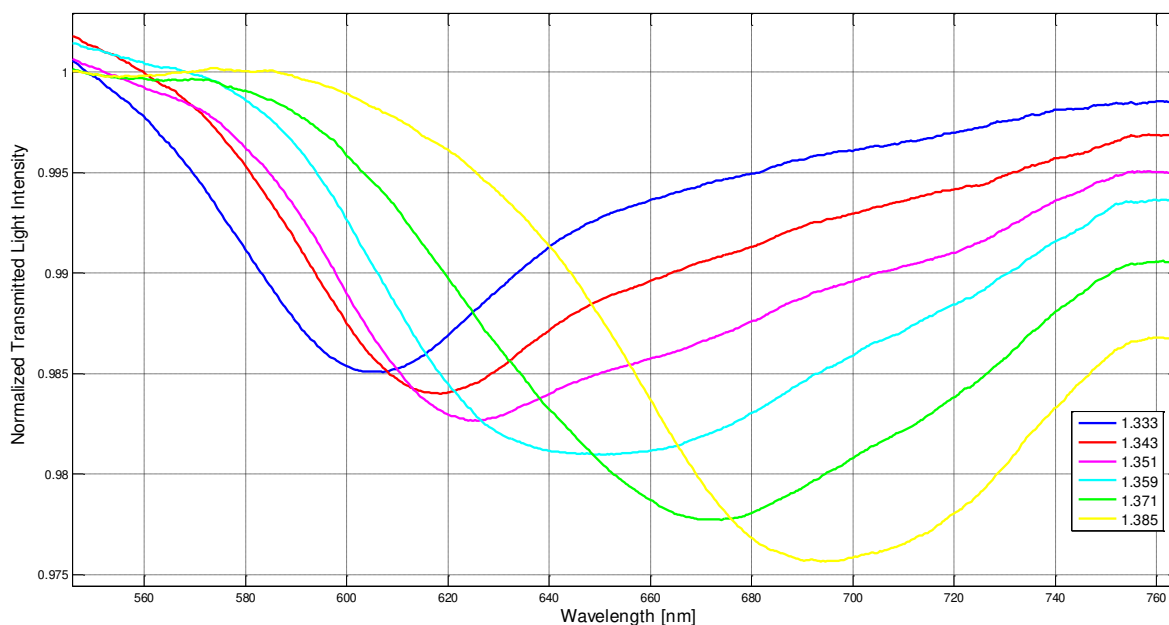

Figure 20. Experimentally obtained SPR transmission spectra, normalized to the air spectrum, for different refractive index of the aqueous medium. Configuration with tapered POF.

Figure 21 shows the resonance wavelength versus the refractive index. In the same figure, it is also presented the linear fitting to the experimental data. The sensitivity, as defined in Equation (2), is the angular coefficient of the linear fitting. Figure 21 shows as the sensitivity increases with the tapered POF configuration.

In this case, i.e. tapered POF without photoresist buffer layer, the sensitivity is about $2*10^3$ (nm/RIU), and it is doubled with respect to the case without tapered POF configuration.

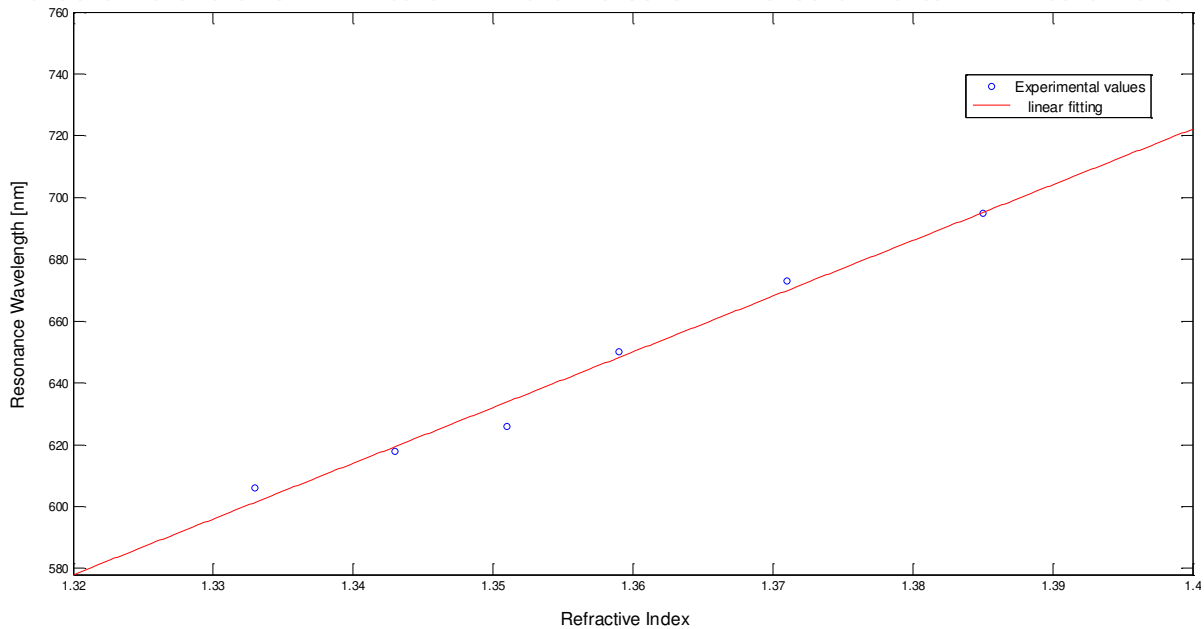**Figure 21.** Plasmon resonance wavelength as a function of the refractive index. Configuration with tapered POF

6. SPR for detection of Bio/chemical Analytes

When artificial receptors are used for Bio/chemicals detection, the film on the surface of metal selectively recognizes and captures the analyte present in a liquid sample so producing a local increase in the refractive index at the metal surface.

The refractive index change Δn_s induced by the analyte molecules binding to the biorecognition elements can be expressed as [10]:

$$\Delta n_s = \left(\frac{dn}{dc} \right)_{vol} \Delta c_s \qquad (10)$$

where $(dn/dc)_{vol}$ is the volume refractive index increment, and Δc_s is the concentration variation of bound analyte expressed in mass/volume or in any other concentration units in the polymer

phase. The value of the refractive index increment depends on the structure of the analyte molecules [11,12].

The refractive index increase gives rise to an increase in the propagation constant of SPW propagating along the metal surface which can be accurately measured, as previously stated.

For this bio-chemical optical sensor with spectral interrogation, the sensitivity is more conveniently defined as:

$$S = \frac{\delta \lambda_{res}}{\delta C} \left[\frac{nm}{M} \right]$$

(11)

In other words, the sensitivity can be defined by calculating the shift in resonance wavelength per unit change in analyte concentration (nm/M).

7. Conclusions

In this chapter we have presented an analysis of SPR phenomenon, a POF sensor based on SPR with the related experimental configurations, a performance comparison of sensors based on SPR in POF and a possible implementation as biosensors. The presented devices are based on the excitation of surface plasmons at the interface between an under test medium (aqueous medium) and a thin planar gold layer deposited on a modified plastic optical fiber. Therefore, the proposed sensing head, being low cost and relatively easy to realize, may be very attractive for bio/chemical sensor implementation [6,7].

Author details

Nunzio Cennamo and Luigi Zeni

Department of Industrial and Information Engineering, Second University of Naples, Aversa, Italy

References

[1] J. Homola, Present and future of surface plasmon resonance biosensors, Anal. Bioanal. Chem. 377, (2003) 528–539.

[2] R.C. Jorgenson, S.S. Yee, A fiber-optic chemical sensor based on surface plasmon resonance, Sens. Actuators B: Chem. 12, (1993) 213–220.

[3] M. Kanso, S. Cuenot, G. Louarn, Sensitivity of optical fiber sensor based on surface plasmon resonance: Modeling and experiments, Plasmonics 3, (2008) 49–57.

[4] N. Cennamo, D. Massarotti, L. Conte, L. Zeni, Low cost sensors based on SPR in a plastic optical fiber for biosensor implementation, Sensors 11, (2011) 11752–11760.

[5] N. Cennamo, D. Massarotti, R. Galatus, L. Conte, L. Zeni, Performance Comparison of Two Sensors Based on Surface Plasmon Resonance in a Plastic Optical Fiber, Sensors 13, (2013) 721-735.

[6] N. Cennamo, A. Varriale, A. Pennacchio, M. Staiano, D. Massarotti, L. Zeni, S. D'Auria, An innovative plastic optical fiber-based biosensor for new bio/applications. The Case of Celiac Disease, Sens. Actuators B: Chem. 176, (2013) 1008–1014.

[7] N. Cennamo, M. Pesavento, G. D'Agostino, R. Galatus, L. Bibbò, L. Zeni, Detection of trinitrotoluene based on SPR in molecularly imprinted polymer on plastic optical fiber, Proceedings of SPIE 0277-786X, V. 8794, Fifth European Workshop on Optical Fibre Sensors, Kraków, Poland 19-22 May 2013

[8] Dwivedi, Y.S.; Sharma, A.K.; Gupta, B.D. Influence of design parameters on the performance of a SPR based fiber optic sensor. Plasmonics 2008, 3, 79–86

[9] R. K. Verna, A. K. Sharma, B. D. Gupta, Modeling of Tapered Fiber-Optic Surface Plasmon Resonance Sensor With Enhanced Sensitivity, IEEE Photonics Technology Letters, VOL. 19, NO. 22, (2007) 1786- 1788.

[10] J. Homola, Surface Plasmon Resonance Based Sensors, Springer Series on Chemical Sensors and Biosensors, Springer-Verlag, Berlin-Heidelberg-New York, 2006

[11] A. Abbas, M. J. Linman, Q. Cheng, New trends in instrumental design for surface plasmon resonance-based biosensors, Biosensors and Bioelectronics 26, (2011) 1815–1824.

[12] S. Scarano, M. Mascini, A. P.F. Turner, M. Minunni, Surface plasmon resonance imaging for affinity-based biosensors, Biosensors and Bioelectronics 25, (2010) 957–966.